Online Impedance Adaptation Facilitates Manipulating a Whip

Xiaofeng Xiong[1], Moses C. Nah[2], Aleksei Krotov[3] and Dagmar Sternad[4]

***Abstract*— Manipulation of flexible objects is one of the major challenges in robotics as the nonlinear dynamics of the high-dimensional object structure makes it difficult to apply current control methods. A previous simulation study showed that control with few pre-structured joint trajectories coupled with joint impedance (dynamic primitives) could control a 25-dimensional whip to hit a target. This was possible even though the impedance values were constant. This paper explores whether time-varying impedance throughout the movement may further enhance performance. We present an online impedance adaptation (OIA) controller that modulates the joint impedances of a two-joint actuator in real time for the same task. Results showed that the OIA control method increased the speed of optimization and resulted in smaller deviation from the zero-torque joint trajectories compared to the controller with constant joint impedances. This novel way to modulate both motion and impedance of a manipulator may facilitate the control of flexible objects with significant dynamics.**

I. Introduction

A prominent challenge in robotics is the manipulation of flexible objects [1]. The complex and nonlinear dynamics originating from the high - in principle infinite - dimensional structure makes it difficult to apply state-of-the-art control methods, which have been developed for rigid object manipulation [2]. It is well recognized that the computational complexity of the task grows exponentially with system dimension, and the optimization quickly becomes intractable – Bellman's "curse of dimensionality" [3]. Several attempts have been made to simplify the problem. One avenue was to replace the full model by a finite lumped-parameter model and then apply optimization-based approaches [4]. Another line of studies in human motor control proposed that a controller based on dynamic primitives is a plausible way to control complex actions, including interacting with the environment [5]–[12].

Specifically, Hogan and Sternad proposed three dynamic primitives: submovements, oscillations and impedances [5]. Using manipulation of a whip as example, Nah et al. demonstrated the benefits of this approach. The authors developed a controller composed of simple pre-shaped joint trajectories (minimum jerk profiles, or submovements) coupled with impedances at each joint of a two-link actuator [13]–[16]. The simulation study tested whether the actuator could hit a distant target with the tip of the whip, when controlled by simple bell-shaped profiles that served as zero-torque trajectories for each of the two joints. At each joint, there was an impedance with constant values of stiffness and damping. The off-line optimization converged to a successful movement of the 10, 15, 20 and 25-link chain models of the whip, without the need of a detailed model of the whip dynamics. This approach highlighted the advantages of primitive components for the control of a high-dimensional flexible object.

While this approach was effective, other studies highlighted the benefits of modulated impedance for physical interaction. For instance, time-varying joint impedances for a 14-DOF Baxter Robot enabled a smooth transition from free motion to contact [17]. Other examples can be found in robotics [17]–[19], human-robot interaction [20]–[22] and human motor control [23]–[26].

Therefore, coupling control via dynamic primitives with varying impedance may improve the efficiency of the optimization and lead to better task performance.

In this paper, we extended the work done in [13] by replacing the constant impedance with an online impedance adaptation (OIA) controller [18], [27]. This extension was tested in three multiple-DOF (i.e., 10, 15, 25) whip models, manipulated by the same two-joint arm. Results showed that OIA control led to faster task optimization and smaller joint position tracking errors compared to corresponding simulations with constant joint impedances [13]. This approach provides a novel way to optimize the movement of a manipulator and facilitate manipulation of complex objects.

II. Methods

All of the simulations were conducted with MuJoCo [28]. The semi-implicit Euler method was chosen as the numerical integrator with a time step of 0.1 $[ms]$.

A. Modeling

A two-joint upper-limb model (the manipulator) and an N-node whip model (the manipulated object) were used for the simulation. The geometrical and inertial parameters of the planar actuator, developed in [13], were borrowed from Hatze [29].

[1]Xiaofeng Xiong is with SDU Biorobotics, the Mærsk Mc-Kinney Møller Institute, University of Southern Denmark, Odence, Denmark, supported by the Human Frontier Science Program, Brødrene Hartmanns, and Thomas B. Thriges, RGP 0002/2017, A36775, and 7648-2106. xizi@mmmi.sdu.dk

[2]Moses C. Mah is with the Department of Mechanical Engineering, Massachusetts Institute of Technology, Cambridge, MA, USA, supported in part by NSF M3X-1826097 (Neville Hogan). mosesnah@mit.edu

[3]Aleksei Krotov is with the Department of Bioengineering, Northeastern University, Boston, MA, USA, supported by NSF M3X-1825942 (Dagmar Sternad). krotov.a@northeastern.edu

[4]Dagmar Sternad is with the Departments of Biology, Electrical & Computer Engineering, and Physics, Northeastern University, Boston, MA, USA, supported in part by NSF M3X-1825942 (Dagmar Sternad) and NIH-R01-HD087089. d.sternad@northeastern.edu

The continuous dynamics of the whip was discretized to an N-node lumped-parameter model. A single sub-model of the whip was comprised of an (ideal) point-mass and a rotational joint. Each point-mass m $[kg]$ was suspended from a massless cylinder with length l $[m]$; the rotational joints consisted of a linear rotational spring and a linear rotational damper with coefficients k $[N \cdot m/rad]$ and b $[N \cdot m \cdot s/rad]$, respectively [13], [14]. The N sub-models were serially connected in a chain-like manner resulting in a N-node whip model. The parameters (N, l, m, k, b) are the "whip parameters" of the N-node whip model. Three whip models were constructed (Table I): short, medium and long, where the parameters of the latter one were experimentally measured from a real bullwhip [13], [16].[1]

TABLE I: Model parameters of the whip

	Whip Parameters				
	N	*l*	*m*	*k*	*b*
Short whip	10	0.1	0.1	0.050	0.005
Medium whip	15	0.1	0.1	0.050	0.005
Long whip	25	0.072	0.012	0.242	0.092

The upper limb was connected to the whip by a freely-rotating hinge joint, i.e., no stiffness or damping elements were included for the handle. The combined model resulted in a sequential open-chain planar mechanism with $(N+2)$-DOFs.

B. Upper-Limb Controller

1) Impedance Controller

A first-order impedance controller with gravity compensation was used for the 2-DOF upper-limb model [13]:

$$\boldsymbol{\tau} = \boldsymbol{K}\left(\boldsymbol{q}_d - \boldsymbol{q}\right) + \boldsymbol{B}\left(\dot{\boldsymbol{q}}_d - \dot{\boldsymbol{q}}\right) + \boldsymbol{\tau}_G \tag{1}$$

where torque $\boldsymbol{\tau}_G(t) \in \mathbb{R}^2$ denotes the torque required for gravity compensation (Sec. II-B.2); $\boldsymbol{q}(t) \in \mathbb{R}^2$ denotes joint displacement vector of the upper-limb model; $\boldsymbol{q}_d(t) \in \mathbb{R}^2$ denotes the "zero-torque" trajectory [13], i.e., neglecting gravitational effects. When the actual joint trajectory $\boldsymbol{q}$ exactly matches the zero-torque trajectory $\boldsymbol{q}_d$, then zero torque is exerted by the joint actuators (Sec. II-B.3); $\boldsymbol{K}(t) \in \mathbb{R}^{2\times2}$ and $\boldsymbol{B}(t) \in \mathbb{R}^{2\times2}$ are the time-varying stiffness and damping matrices representing the neuromuscular impedances of the upper-limb segments, respectively; the impedance matrices $\boldsymbol{K}(t)$ and $\boldsymbol{B}(t)$ are online adapted via the OIA control law (Sec. II-B.4);

2) Gravity Compensation

Gravitational effects of the model were compensated with $\boldsymbol{\tau}_G(t)$, such that the actual upper-limb posture $\boldsymbol{q}$ exactly matched the zero-torque posture $\boldsymbol{q}_d$ when the whole model was at rest [14]:

$$\boldsymbol{\tau}_G = \boldsymbol{J}_1^T \boldsymbol{f}_1 + \boldsymbol{J}_2^T \boldsymbol{f}_2 + \boldsymbol{J}_3^T \boldsymbol{f}_3 \tag{2}$$

[1]The experimentally-fitted whip model constructed in [13] corresponds to the long whip model.

where $\boldsymbol{J}_{1-3} \in \mathbb{R}^{3\times2}$ are the Jacobian matrices in terms of the center of mass of the upper arm, center of mass of the forearm, and the end-effector with respect to the frame attached to the shoulder, respectively.

$\boldsymbol{f}_{1-3} \in \mathbb{R}^3$ denote the gravitational forces due to the mass of the upper arm, forearm, and whip model, respectively [14]:

$$\boldsymbol{f}_1 = M_1\boldsymbol{g}, \;\; \boldsymbol{f}_1 = M_2\boldsymbol{g}, \;\; \boldsymbol{f}_3 = M_w\boldsymbol{g} \tag{3}$$

where $M_1 = 0.291$ $[kg]$ and $M_2 = 0.294$ $[kg]$ denote the mass of the upper arm and forearm, respectively [13]; M_w denotes the total mass of the whip model, which is equal to the node number of the whip N times the mass of each sub-model m ($M_w = N \cdot m$); $\boldsymbol{g} \in \mathbb{R}^3$ denotes gravity in the simulation environment.

3) Zero-Torque Trajectory

The zero-torque trajectory of the controller, $\boldsymbol{q}_d(t)$ (Eq. 1) followed a minimum-jerk trajectory [13], [30]:

$$\boldsymbol{q}_d(t) = \boldsymbol{q}_i + (\boldsymbol{q}_f - \boldsymbol{q}_i)\left\{10\left(\frac{t}{D}\right)^3 - 15\left(\frac{t}{D}\right)^4 + 6\left(\frac{t}{D}\right)^5\right\} \tag{4}$$

where $\boldsymbol{q}_i = [q_{i,s}, q_{i,e}]^T$ $[rad]$ and $\boldsymbol{q}_f = [q_{f,s}, q_{f,e}]^T$ $[rad]$ denote the initial and final zero-torque joint posture, respectively; D $[s]$ is the duration of the trajectory; subscripts s and e denote shoulder and elbow joints, respectively. For times longer than the duration D (i.e. $t > D$), the zero-torque trajectory $\boldsymbol{q}_d(t)$ remained at $\boldsymbol{q}_f$ [13].

4) Online Impedance Adaptation (OIA)

The elements of the joint stiffness matrix $\boldsymbol{K}(t)$ and damping matrix $\boldsymbol{B}(t)$ of the impedance controller were modulated in real time:

$$\boldsymbol{K}(t) = \begin{bmatrix} k_{ss}(t) & k_{se}(t) \\ k_{es}(t) & k_{ee}(t) \end{bmatrix}, \; \boldsymbol{B}(t) = \begin{bmatrix} b_{ss}(t) & b_{se}(t) \\ b_{es}(t) & b_{ee}(t) \end{bmatrix} \tag{5}$$

where $k(t)$ and $b(t)$ are the stiffness and damping parameters of the upper-limb model [31]; subscript s and e correspond to the shoulder and elbow joints, respectively; diagonal and off-diagonal terms correspond to the impedances arising from the monoarticular and biarticular muscles of the upper limb, respectively (Fig. 1).

The adaptation law of the impedance matrices $\boldsymbol{K}(t)$ and $\boldsymbol{B}(t)$ minimized the following scalar cost function J:

$$J = J_c + J_p \tag{6}$$

The cost function J_c was defined as follows:

$$J_c = \frac{1}{2}\int_0^D \left(\|vec(\tilde{\boldsymbol{K}})\|^2_{\boldsymbol{Q_K}} + \|vec(\tilde{\boldsymbol{B}})\|^2_{\boldsymbol{Q_B}}\right)d\tau \tag{7}$$

which is the time integration of the weighted norms of matrices $\tilde{\boldsymbol{K}}$, $\tilde{\boldsymbol{B}} \in \mathbb{R}^{2\times2}$ from the start to the end of the zero-torque trajectory (Eq. 4); $\|\cdot\|_{\boldsymbol{Q_K},\boldsymbol{Q_B}}$ and $vec(\cdot)$ denote the weighted norms and column vectorization, respectively; $\boldsymbol{Q_K} \in \mathbb{R}^{4\times4}$ and $\boldsymbol{Q_B} \in \mathbb{R}^{4\times4}$ are positive symmetric weighting matrices, where the norm of the matrix affects the speed of optimization [18]; $\tilde{\boldsymbol{K}}$ and $\tilde{\boldsymbol{B}}$ are defined as the difference between the actual and expected values of the stiffness and damping matrices [18]:

$$\tilde{\boldsymbol{K}} = \boldsymbol{K} - \boldsymbol{K}_E, \;\; \tilde{\boldsymbol{B}} = \boldsymbol{B} - \boldsymbol{B}_E \tag{8}$$

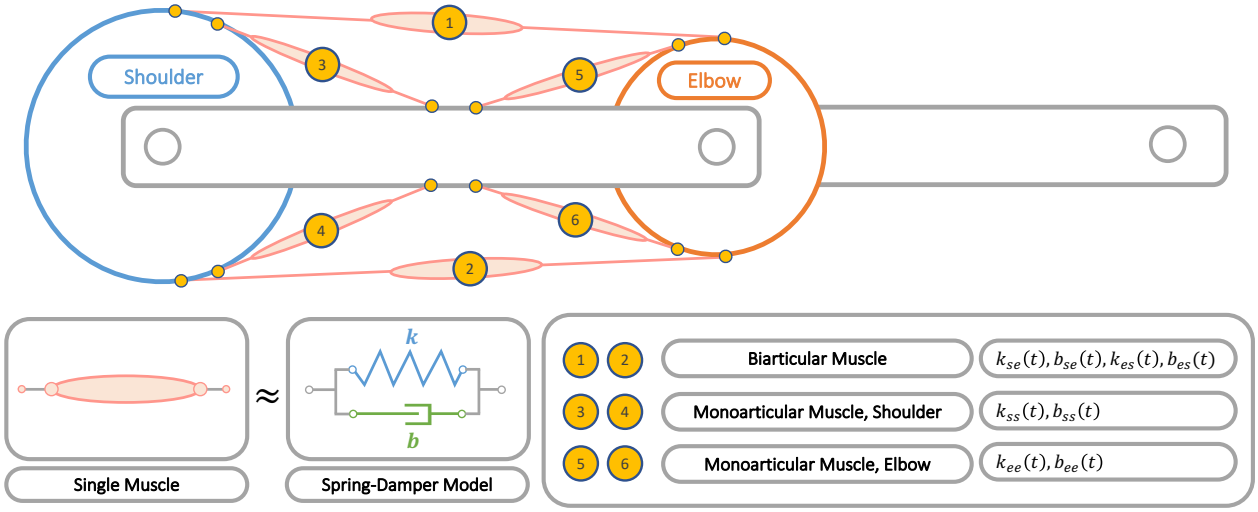

Fig. 1: Muscle model of the two-joint upper limb showing the monoarticular and biarticular muscles of the shoulder and elbow joints.

where subscript $\boldsymbol{K}_E$ and $\boldsymbol{B}_E$ denote the impedance (matrices) to ensure movement stability (i.e., Eq. 13), from which the optimal $\boldsymbol{K}$ and $\boldsymbol{B}$ are optimized.

The cost function J_p is defined as follows:

$$J_p = \int_0^D \dot{V}(\tau)d\tau,\ V(t) = \frac{1}{2}\boldsymbol{\varepsilon}^T(t)\boldsymbol{I}(\boldsymbol{q})\boldsymbol{\varepsilon}(t) \tag{9}$$

where the integrand is the time differentiation of the scalar function $V(t)$, integrated from start to the end of the zero-torque trajectory (Eq. 4); $\boldsymbol{I}(\boldsymbol{q}) \in \mathbb{R}^{2\times 2}$ is the inertia matrix of the 2-DOF upper-limb model; $\boldsymbol{\varepsilon}(t)$ is the time-varying sliding variable [32], defined as follows:

$$\boldsymbol{\varepsilon}(t) = \boldsymbol{e}(t) + \beta\dot{\boldsymbol{e}}(t),\ \boldsymbol{e}(t) = \boldsymbol{q}_d(t) - \boldsymbol{q}(t) \tag{10}$$

where $\boldsymbol{e}(t) \in \mathbb{R}^2$ is the tracking error between the zero-torque trajectory and the actual joint trajectory of the upper-limb model; β is a positive constant.

The resulting adaptation law of the impedances that minimized the cost function J is as follows [18]:

$$\boldsymbol{K}(t) = \boldsymbol{F}(t)\boldsymbol{e}^T(t),\ \boldsymbol{B}(t) = \boldsymbol{F}(t)\dot{\boldsymbol{e}}^T(t),\ \boldsymbol{F}(t) = \frac{\boldsymbol{\varepsilon}(t)}{\gamma(t)} \tag{11}$$

where $\gamma(t)$ is an adaptation scalar defined as:

$$\gamma(t) = \frac{a}{1 + C\|\boldsymbol{\varepsilon}(t)\|^2}. \tag{12}$$

The values of the positive scalars used for the simulation are $a = 0.2$ and $C = 5$. They were chosen to ensure online stable adaptation control. Further details and stability proof of the online impedance adaptation law (Eq. 11) were presented in [18].

C. Task Definition and Optimization

The whip task was defined to evaluate the performance of the upper-limb movement guided by the suggested controller. The task objective was to hit a distant target with a whip (Fig. 2). That objective was quantified as minimizing the distance between the tip of the whip and target, L $[m]$. The target was located at shoulder height 0.01 $[m]$ beyond the whip range [13]. Three whip models — the short, medium and long whip model (Table I) — were tested.

To demonstrate the effectiveness of the OIA control law, it was compared to a controller with constant joint impedance parameters [13]. The controller with constant impedance parameters is referred to as "ZTTO" (zero-torque trajectory optimization) controller, and the controller which adds the online impedance adaption (OIA) law is referred to as "ZTTO+OIA" controller.

For the ZTTO controller, submovement parameters of the zero-torque trajectory $(q_{i,s},\ q_{i,e},\ q_{f,s},\ q_{f,e},\ D)$ (Eq. 4) were optimized using the "Dividing rectangles-locally biased" (DIRECT-L) algorithm in the "nonlinear optimization Python tool box" (nlopt) [33]. In the ZTTO+OIA controller joint impedances were modulated in real time after each iteration of the submovement optimization using DIRECT-L (Eq. 11). The optimization was terminated when the distance L was lower than the threshold value $L_d = 0.10$ $[m]$, i.e., **Min**(L^*) $< L_d$ (**Algorithm 1**). The obtained minimal distance, L^* $[m]$, determined the performance.

III. Results

For all three whip models, the proposed ZTTO+OIA approach outperformed the ZTTO approach in the following aspects (see also the experimental video[2]):

1) Faster Task Optimization

The ZTTO+OIA controller reached the threshold value $L_d = 0.10$m in fewer iterations than the ZTTO controller; the improvement was roughly a factor of 2 (Fig. 3).

2) Smaller Tracking Errors

The ZTTO+OIA controller reached smaller tracking errors of joint positions, indicating better tracking of the zero-torque trajectory (Fig. 4C, 4E).

3) Time-Varying Impedance

The ZTTO+OIA controller rendered time-varying joint impedance of the upper-limb model with average stiffness

[2] https://www.youtube.com/watch?v=AV_7qP6Yd-Y

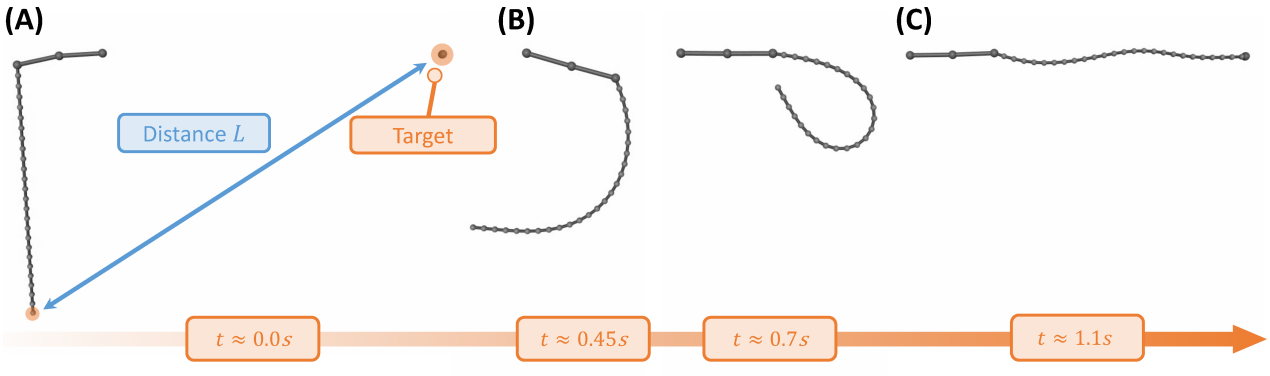

Fig. 2: Time sequence of the simulation using the long whip model (see Table I). (A) Beginning of the movement, (B) Intermediate movement phase and the final arm posture, (C) Whip reaching the minimal distance to the target.

Algorithm 1: Optimization of the whip task

Inputs: L_d = 0.10m (threshold distance);
Outputs: Optimal $(q_{i,s},\ q_{i,e},\ q_{f,s},\ q_{f,e},\ D)$ (Eq. 4);
Optimization initialization, $t_0 = 0.05$ $[s]$, $T = 1.2$ $[s]$;
for *DIRECT-L, i = 1 to 600* **do**
  Simulation initialization;
  Update $(q_{i,s},\ q_{i,e},\ q_{f,s},\ q_{f,e},\ D)$ (Eq. 4);
  while $0 \leq t < T$ **do**
    Compute $\boldsymbol{\tau}_G$ (Eq. 2);
    while $t_0 \leq t < t_0 + D$ **do**
      Compute $\boldsymbol{q}_d$, $\dot{\boldsymbol{q}}_d$, $\boldsymbol{e}$, $\dot{\boldsymbol{e}}$ (Eq. 4 and 10);
      if *OIA == True* **then**
        Update $\boldsymbol{K}$ and $\boldsymbol{B}$ (Eq. 11);
      else
        Use constant $\boldsymbol{K}$ and $\boldsymbol{B}$ (Eq. 13);
      end
    end
    Compute/command torque inputs $\boldsymbol{\tau}$ (Eq. 1);
    Compute and save distance L;
  end
  Save $L^* = \boldsymbol{Min}$(L);
  if $\boldsymbol{Min}(L^*) < L_d$ **then**
    break;
  end
end
Save the performance $\boldsymbol{Min}(L^*)$ and movement parameters $[q_{i,s}, q_{i,e}, q_{f,s}, q_{f,e}, D]^T$;

smaller and average damping larger than the ZTTO controller (Fig. 5).

IV. Discussion

This study attempted to emphasize the beneficial role of varying mechanical impedance for physical interaction in the context of complex object manipulation. The simulation presents a novel optimization of both motion and impedance of an actuator when manipulating a whip — one of the most complex tools that humans can handle. Manipulating a whip

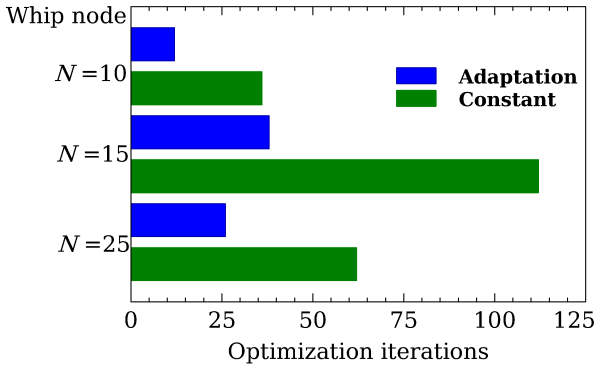

Fig. 3: Number of iterations before reaching the threshold distance between whip and target $L_d = 0.1$ $[m]$. ZTTO controller assumed constant impedances, while ZTTO+OIA controller modulated impedances.

is one example for the challenges that soft robotics faces. Not only did the controller optimize the parameters of the submovements of the joints (the ZTTO part of the proposed algorithm), it also modulated the mechanical impedances in real time (the OIA part) (Fig. 5). Adding OIA resulted in faster optimization and smaller joint tracking errors.

The impedance values identified by the OIA method showed that joint stiffness increased during the early part of the arm movement, from 0 to 0.45 $[s]$ (see Fig. 2), and then dropped rapidly, approaching near-zero values by the end of the movement (around 0.7 $[s]$), for all three whip models. The time profile of damping was less regular, but also exhibited a rapid decrease shortly before 0.45 s. By that time, the manipulator had nearly reached its terminal configuration while the whip had gained a high speed moving upwards and unfolding towards the target. The fact that the tracking error was lower in ZTTO+OID (Fig. 4) indicates a shift of the controller's priority from position toward force control – such shift being likely related to the whip dynamics.

Across the three whip models, larger average stiffness and damping were observed for the long whip model (Fig. 5). This is likely due to its mechanical properties that were taken from a real bullwhip; that whip was lighter, stiffer and more viscous than the other two models [13], [16]. In-depth

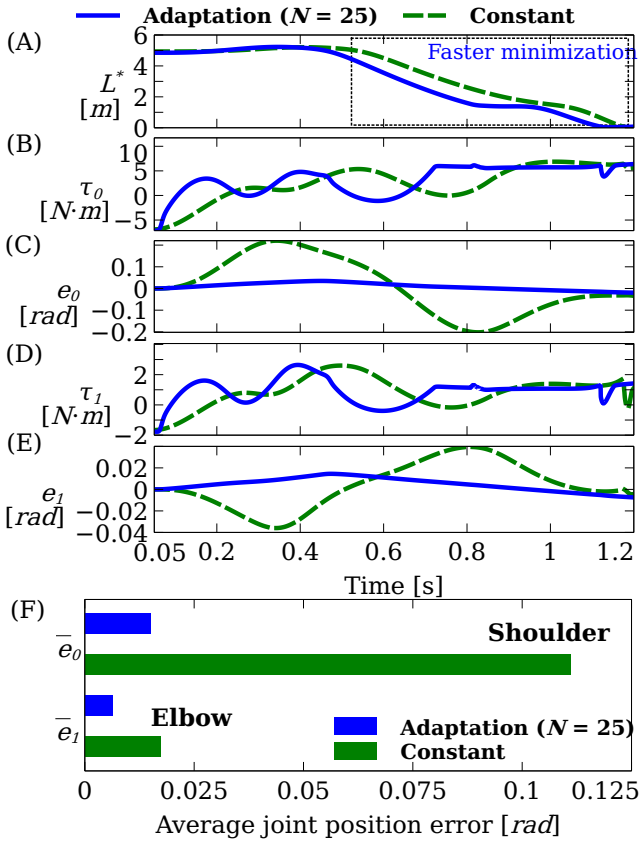

Fig. 4: Task-specific parameters during execution using the long whip model, with the ZTTO (green) and the ZTTO+OIA (blue) controllers. (A) Distance L between the whip and target. (B,C) Net torque input τ_s and position error e_s of the shoulder joint. (D,E) Net torque input τ_e and position error e_e of the elbow joint. The movement started at 0.05 [s] (Algorithm 1). (F) Average joint position error of each joint.

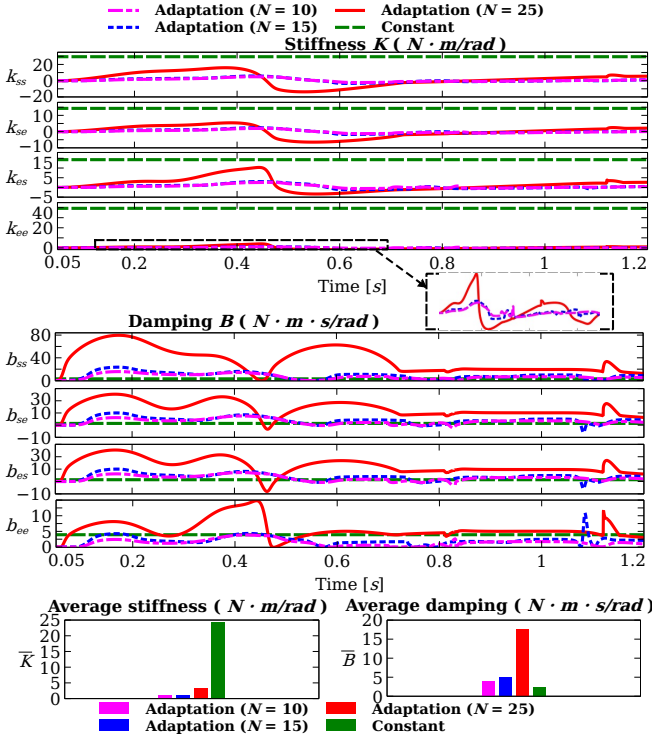

Fig. 5: Time vs. elements of impedance matrices $\boldsymbol{K}$ and $\boldsymbol{B}$ using the ZTTO+OIA controller (Eq. 5). The simulation was generated by the optimal movement parameters of each whip model. Time -varying impedances (blue) compared with the constant impedance value (green) used in the ZTTO controller (Eq. 13). Average stiffness $\overline{\boldsymbol{K}}$ and average damping $\overline{\boldsymbol{B}}$ (Eq. 15) for each whip model, compared with the constant impedance value (green).

analysis of the whip properties may provide further insights into the relation of whip model and the resulting controller impedance.

Modulating impedance was previously suggested to facilitate robot interaction with environment, particularly its transition between free motion and contact [17], [19], [21]. In addition, Braun et al. suggested increased efficiency, as varying impedance improves energy storage capabilities of the manipulator [21].

The simulations showed that stiffness could occasionally reach negative values (Fig. 5). Similar negative values also emerged in several robotic applications of time-varying impedance [18], [21], [27]. While negative stiffness is generally understood to jeopardize controller stability, it was previously shown that the present method can maintain stability [18], provided properly selected adaptation scalar and weighting norms for stiffness and damping matrices.

The whip manipulation task is inspired by human performance. Most of impedance-related studies in humans examined much simpler tasks such as static postures, reaching, walking, and ball-catching. For example, arm joint impedance was examined in static postures as it allowed for careful perturbations, [31], [34], [35]. While rigorous measurement of joint impedance remains a known hurdle [36], [37], several studies have reported varying impedance during volitional movements. Lacquaniti et al. observed varying impedance in the human arm during catching a ball and suggested independent control of stiffness, inertia and damping of the arm by the central nervous system [24]. In the ankle, similar variation of impedance was suggested to facilitate muscle efficiency while walking [23], [25]. Furthermore, Dyhre-Poulsen et al. studied landing after a jump and reported negative stiffness in the ankle, suggesting that this might facilitate damping by the soleus muscle [26]. Rouse et al. suggested that negative viscosity in the ankle may facilitate energy storage during the early stance phase [25]. Aside from these observations in humans, negative damping was found to facilitate generalization motor skill in humans and also facilitate human-robot interaction [20], [22]. The time-varying impedance of the manipulator may be an efficient means of improving energy-storing capabilities of the robot and facilitating its interaction with external objects.

While some promising implementations of the OIA controller have already been reported [18], [27], [38], more rigorous evaluation of these conjectures are needed. In movement neuroscience it remains to be an important goal to develop experimental paradigms that study human interaction with real-world complex objects [16]. Such investigation may reveal further information for both neuroscience and robotics.

APPENDIX

The joint stiffness matrix $\boldsymbol{K} \in \mathbb{R}^{2\times 2}$ and damping matrix $\boldsymbol{B} \in \mathbb{R}^{2\times 2}$ used for the ZTTO controller are given by [13]:

$$\boldsymbol{K} = \begin{bmatrix} 29.5 & 14.3 \\ 14.3 & 39.3 \end{bmatrix}, \quad \boldsymbol{B} = 0.1\boldsymbol{K} = \begin{bmatrix} 2.95 & 1.43 \\ 1.43 & 3.93 \end{bmatrix} \tag{13}$$

The average values of the joint stiffness $\overline{\boldsymbol{K}}$ and damping matrices $\overline{\boldsymbol{B}}$ are calculated as follows:

$$\overline{\boldsymbol{K}} = \frac{1}{4}\sum_{i=0}^{3}\left(\frac{\sum_{j=0}^{N}|vec(\boldsymbol{K})_i(t_0 + j\cdot\Delta T)|}{N}\right), \tag{14}$$

$$\overline{\boldsymbol{B}} = \frac{1}{4}\sum_{i=0}^{3}\left(\frac{\sum_{j=0}^{N}|vec(\boldsymbol{B})_i(t_0 + j\cdot\Delta T)|}{N}\right) \tag{15}$$

where $t_0 = 0.05$ $[s]$ is the time when the movement starts, $\Delta = 0.1$ $[ms]$ is the time step of the simulation and N is the number of samples collected from start to end of zero-torque trajectory with duration D, i.e., $N = D/\Delta T$.

ACKNOWLEDGMENT

The authors would like to thank Anders Lyhne Christensen for support and consulting during this work.

REFERENCES

[1] A. Billard and D. Kragic, "Trends and challenges in robot manipulation," *Science*, vol. 364, no. 6446, 2019.

[2] O. M. Andrychowicz, B. Baker, M. Chociej, R. Jozefowicz, B. McGrew, J. Pachocki, A. Petron, M. Plappert, G. Powell, A. Ray, *et al.*, "Learning dexterous in-hand manipulation," *The International Journal of Robotics Research*, vol. 39, no. 1, pp. 3–20, 2020.

[3] R. E. Bellman, *Adaptive control processes: a guided tour*, vol. 2045. Princeton university press, 2015.

[4] E. Papadopoulos, F. Aghili, O. Ma, and R. Lampariello, "Robotic manipulation and capture in space: A survey," *Frontiers in Robotics and AI*, vol. 8, p. 228, 2021.

[5] N. Hogan and D. Sternad, "Dynamic primitives of motor behavior," *Biological Cybernetics*, vol. 106, no. 11, pp. 727–739, 2012.

[6] N. Hogan, "Physical interaction via dynamic primitives," in *Geometric and Numerical Foundations of Movements* (J.-P. Laumond, N. Mansard, and J.-B. Lasserre, eds.), pp. 269–299, Springer International Publishing, 2017.

[7] H. Guang, S. Bazzi, D. Sternad, and N. Hogan, "Dynamic primitives in human manipulation of non-rigid objects," in *2019 IEEE International Conference on Robotics and Automation*, pp. 3783–3789, 2019.

[8] R. Nayeem, S. Bazzi, N. Hogan, and D. Sternad, "Transient behavior and predictability in manipulating complex objects," in *2020 IEEE International Conference on Robotics and Automation*, pp. 10155–10161, 2020.

[9] S. Bazzi and D. Sternad, "Robustness in human manipulation of dynamically complex objects through control contraction metrics," *IEEE Robotics and Automation Letters*, vol. 5, pp. 2578–2585, 2020.

[10] S. Schaal, "Dynamic movement primitives - a framework for motor control in humans and humanoid robotics," in *Adaptive Motion of Animals and Machines* (H. Kimura, K. Tsuchiya, A. Ishiguro, and H. Witte, eds.), pp. 261–280, Tokyo: Springer-Verlag, 2006.

[11] N. Hogan and D. Sternad, "Dynamic primitives in the control of locomotion," *Frontiers in Computational Neuroscience*, vol. 9, pp. 2002–2005, 2013.

[12] D. Sternad, W. J. Dean, and S. Schaal, "Interaction of rhythmic and discrete pattern generators in single-joint movements," *Human Movement Science*, vol. 19, no. 4, pp. 627–664, 2000.

[13] M. C. Nah, A. Krotov, M. Russo, D. Sternad, and N. Hogan, "Dynamic primitives facilitate manipulating a whip," in *2020 8th IEEE RAS/EMBS International Conference for Biomedical Robotics and Biomechatronics (BioRob)*, pp. 685–691, 2020.

[14] M. C. Nah, *Dynamic primitives facilitate manipulating a whip*. Master of science thesis, Massachusetts Institute of Technology, 2020.

[15] B. Bernstein, D. A. Hall, and H. M. Trent, "On the dynamics of a bull whip," *The Journal of the Acoustical Society of America*, vol. 30, no. 12, pp. 1112–1115, 1958.

[16] A. Krotov, *Human control of a flexible object: hitting a target with a bull-whip*. Master of science thesis, Northeastern University, 2020.

[17] G. Averta and N. Hogan, "Enhancing robot-environment physical interaction via optimal impedance profiles," in *2020 8th IEEE RAS/EMBS International Conference for Biomedical Robotics and Biomechatronics (BioRob)*, pp. 973–980, 2020.

[18] X. Xiong and P. Manoonpong, "Adaptive motor control for human-like spatial-temporal adaptation," in *IEEE International Conference on Robotics and Biomimetics*, pp. 2107–2112, 2018.

[19] D. J. Braun, V. Chalvet, and A. Dahiya, "Positive-negative stiffness actuators," *IEEE Transactions on Robotics*, vol. 35, pp. 162–173, 2019.

[20] T. Bitz, F. Zahedi, and H. Lee, "Variable damping control of a robotic arm to improve trade-off between agility and stability and reduce user effort," in *IEEE International Conference on Robotics and Automation*, pp. 11259–11265, 2020.

[21] D. Braun, M. Howard, and S. Vijayakumar, "Optimal variable stiffness control: formulation and application to explosive movement tasks," *Autonomous Robots*, vol. 33, no. 3, pp. 237–253, 2012.

[22] F. C. Huang, J. L. Patton, and F. A. Mussa-Ivaldi, "Manual skill generalization enhanced by negative viscosity," *Journal of Neurophysiology*, vol. 104, no. 4, pp. 2008–2019, 2010.

[23] H. Lee and N. Hogan, "Time-varying ankle mechanical impedance during human locomotion," *IEEE Transactions on Neural Systems and Rehabilitation Engineering*, vol. 23, no. 5, pp. 755–764, 2014.

[24] F. Lacquaniti, M. Carrozzo, and N. A. Borghese, "Time-varying mechanical behavior of multijointed arm in man," *Journal of Neurophysiology*, vol. 69, no. 5, pp. 1443–1463, 1993.

[25] E. J. Rouse, L. J. Hargrove, E. J. Perreault, and T. A. Kuiken, "Estimation of human ankle impedance during the stance phase of walking," in *IEEE Transactions on Neural Systems and Rehabilitation Engineering*, pp. 870–878, 2014.

[26] P. Dyhre-Poulsen, E. Simonsen, and M. Voigt, "Dynamic control of muscle stiffness and H reflex modulation during hopping and jumping in man," *The Journal of Physiology*, vol. 437, pp. 287–304, jun 1991.

[27] X. Xiong and P. Manoonpong, "Online sensorimotor learning and adaptation for inverse dynamics control," *Neural Networks*, vol. 143, pp. 525–536, 2021.

[28] E. Todorov, T. Erez, and Y. Tassa, "MuJoCo: A physics engine for model-based control," in *2012 IEEE/RSJ International Conference on Intelligent Robots and Systems*, pp. 5026–5033, 2012.

[29] H. Hatze, "A mathematical model for the computational determination of parameter values of anthropomorphic segments," *Journal of Biomechanics*, vol. 13, no. 10, pp. 833–843, 1980.

[30] T. Flash and N. Hogan, "The coordination of arm movements: an experimentally confirmed mathematical model," *Journal of Neuroscience*, vol. 5, no. 7, pp. 1688–1703, 1985.

[31] J. McIntyre, F. A. Mussa-Ivaldi, and E. Bizzi, "The control of stable postures in the multijoint arm," *Experimental Brain Research*, vol. 110, no. 2, pp. 248–264, 1996.

[32] J.-J. E. Slotine, "Sliding controller design for non-linear systems," *International Journal of control*, vol. 40, no. 2, pp. 421–434, 1984.

[33] J. M. Gablonsky and C. T. Kelley, "A locally-biased form of the DIRECT algorithm," *Journal of Global Optimization*, vol. 21, no. 1, pp. 27–37, 2001.

[34] F. Mussa-Ivaldi, N. Hogan, and E. Bizzi, "Neural, mechanical, and geometric factors subserving arm posture in humans," *The Journal of Neuroscience*, vol. 5, no. 10, pp. 2732–2743, 1985.

[35] D. B. Lipps, E. M. Baillargeon, D. Ludvig, and E. J. Perreault, "Quantifying the multidimensional impedance of the shoulder during volitional contractions," *Annals of Biomedical Engineering*, vol. 48, no. 9, pp. 2354–2369, 2020.

[36] J. Mizrahi, "Mechanical impedance and its relations to motor control, limb dynamics, and motion biomechanics," *Journal of Medical and Biological Engineering*, vol. 35, no. 1, pp. 1–20, 2015.

[37] E. J. Rouse, R. D. Gregg, L. J. Hargrove, and J. W. Sensinger, "The difference between stiffness and quasi-stiffness in the context of biomechanical modeling," *IEEE Transactions on Biomedical Engineering*, vol. 60, no. 2, pp. 562–568, 2013.

[38] X. Xiong, F. Wörgötter, and P. Manoonpong, "Adaptive and energy efficient walking in a hexapod robot under neuromechanical control and sensorimotor learning," *IEEE Transactions on Cybernetics*, vol. 46, no. 11, pp. 2521–2534, 2016.